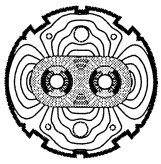

Main Magnets and Superconductors Group
LHC-MMS

Internal Note 97-09

Superconducting Cable Topology

J-M. Depond, D. Leroy and L. Oberli - LHC-MMS

Distribution: LHC-MMS Scientific Staff
J-M. Depond

1. Introduction

The cabling process modifies significantly the shape of strands (initially cylindrical) in the superconducting cables. The internal structure of the cable is only poorly defined by the width, the mid-thickness, the keystone angle, the twist-pitch and the compaction rate. However, a correct estimation of the cable topology is essential to define such fundamental parameters as contact areas or free volumes. We have built a mathematical model to reconstruct from direct measurements an approximated shape of the strand in various superconducting cables. We calculated some key-parameters (contact areas, free volumes, etc.) and discussed their evolution inside the cable. Moreover we determined the effect of compaction on the free volumes inside superconducting cable.

2. Purpose of the study

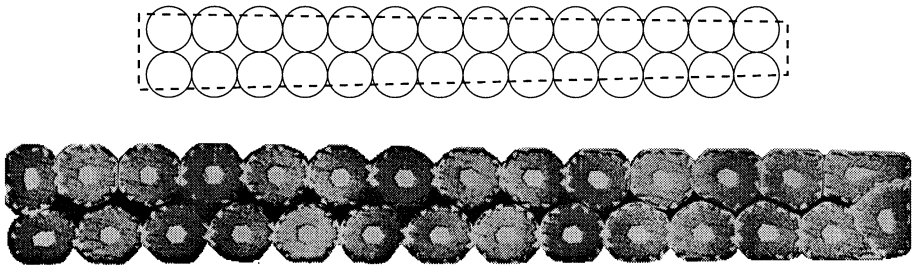

Figure 1: Superconducting cable section before and after cabling

A superconducting cable is composed by twisted superconducting strands in various numbers and various diameters. By forming under pressure, the set of cylindrical strands becomes a strip with a trapezoidal section, characterised by a width, a mid-thickness, a keystone angle and a twist-pitch. During this process, the strand section is mainly deformed (cf fig. 1): strands are squared at the centre of the section cable and triangularised at each end. Plastic deformations appear at each crossing of strands from top and bottom layers and along the strands, increasing the contact areas between neighbours but decreasing the exchange surfaces with liquid helium. Furthermore free volumes are strongly lowered. Those parameters are fundamental to study the stability of superconducting cable but none can be easily measured *in situ*. It is therefore interesting to build a 3D modelling of an extracted strand from 2D measurements in order to calculate with some reasonable accuracy the contact areas, the exchange areas and the free volumes.

We have built such a 3D modelling for 5 different cables given in table A: 4 inner cables from 17 mm to 15 mm width and a 15 mm width outer cable. All of them have been used in a LHC dipole magnet. The samples 2136 and 2180 correspond to the old design (> 15 mm width) but the samples 2191 and 2B164 are typical of the 15 mm width inner and outer cables. The inner cable 1B263 belongs to the new 15.1 mm width design. Parameters of this new design have been chosen by transposing some characteristics of the cable 2180, used in the MFISC magnet, to the 15 mm design: a lower compaction rate specially near the thin edge obtained by increasing the mid-thickness of the 15 mm width cable and by decreasing the keystone angle.

After presenting the 2D measurements technique and the 3D modelling hypotheses, we discuss the calculated values of useful areas and volumes, their evolution along the strand and the effect of compaction and shape parameters.

Table A: Characteristics of studied cables

Cable reference	2136	2180	2191	1B263	2B164
Type	Inner	Inner	Inner	Inner	Outer
Number of strands	26	30	28	28	36
Strand diameter (mm)	1.298	1.097	1.063	1.064	0.826
Width (mm)	17	16.7	15.0	15.1	15.0
Mid-thickness (mm)	2.261	1.959	1.878	1.896	1.467
Keystone angle (°)	1.585	1.178	1.307	1.191	0.979
Twist-pitch length (mm)	130	130	117	114	101
Twist-pitch angle (°)	14.7	14.4	14.4	14.8	16.5
Number of filaments	21780	20328	20328	8874	6408
Filament diameter (µm)	5.4	4.6	7	7	6
Wire surface (mm^2)	14247	13878	11296	11038	9840
Wire volume (mm^3)	4623	3806	3002	2936	2032
Envelope volume (mm^3)	4997	4253	3296	3264	2222
Total free volume (mm^3)	374	447	294	328	190
Compaction rate	92.5 %	89.5 %	91.1 %	90.0 %	91.5 %
Magnet reference	MTP1A1	MFISC	MBSMS5	MBSMS12	MBSMS8

3. Measurement techniques

We use the profile projection technique to obtain a 2D image of the top, back and sides of a strand extracted from a superconducting cable (fig. 2): the sample is lighted by a parallel beam which project a shadow on an optical magnifying device (x 50). This shadow corresponds to the contour of the sample (diascopy technique). Moreover, two halogen spots illuminate the shadowed part of the sample. By playing with the illumination angle, the reflected light, collected by the optical device, gives by contrast an image of the shape of the shadowed part (episcopy technique).

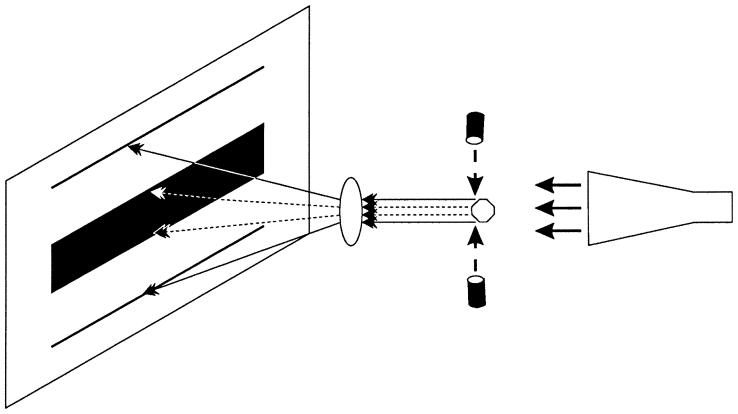

Figure 2: Profile projection technique

Typical projections are presented on figure 3. Image a) shows a top view with a well-defined oval-shaped plastic deformation due to the contact of the top and bottom strands layers inside the cable. Image b) shows a back view with the flattening due to the contact strand/Turk's head roller during

the cable extrusion. Image c) shows a side view with the flattened surface due to the contact between adjacent strands. We also observe the small indentation due to the crossing deformation defined in a) and its limit (dot line). For a correct image of the side view, the projection has to be done following the main axis of the elliptic crossing. Moreover, for a correct delimitation of the contours, it is essential to orient the flattened surfaces as parallel as possible to the diascopy illumination axis: this avoids the supplementary shadows which could be induced by the flattenings.

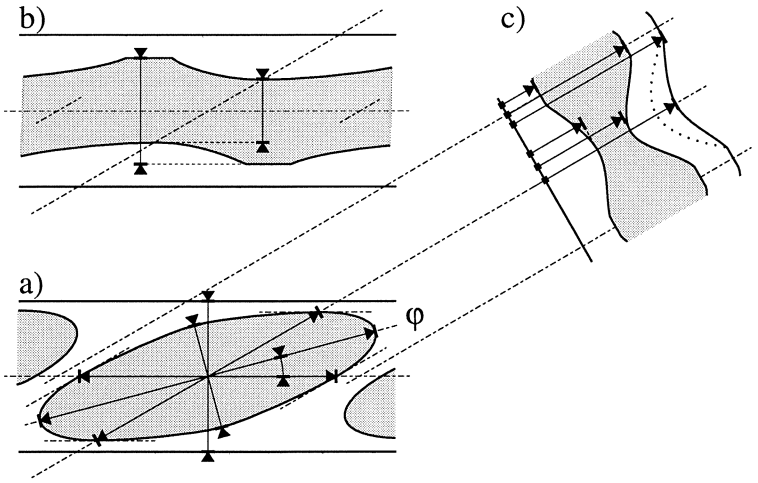

Figure 3: Typical projections : a) top view, b) back view, c) side view.

From those pictures, we extract characteristic distances (represented by arrow line in figures 3) with ±5 μm accuracy in order to build the 3D modelling. They characterise:

- the elliptical crossing area: long and short axes, main axis or eccentricity, main angle (φ) - measured on the top view (a) -;
- the strand: width - measured on the top view (a) or the back view (b) -, heights at the centre of the crossing area and on each side - measured on the side view (c) -;
- the back flattening : minimum and maximum distances between the right and left limits of the flattened surface - measured on the back view (b) -;
- the side flattening: minimum and maximum distances from the bottom of the strand to the lower and upper limits of the flattening - measured on the side view (c) -.

Some of those measurements can be crosschecked in the following way:

- the main angle φ should be equal to the double of the twist-pitch angle, *i. e.* the angle of the wire crossing;
- the strand width measured on the top view should be equal to the one measured on the back view;
- the sum of the strand width is linked to the twist-pitch length by the twist-pitch angle;
- the evolution of the height at the centre of the crossing area should be linear and linked to the mid-thickness and the keystone angle.

4. Topological modelling

From the measurements, we build a topological modelling of the strand in place in the superconducting cable. We neglect first the few μm displacements due to elastic relaxation on each contact surface. So the back flattening and the side flattening of the strands are perfectly flat. Their

limits are assumed to be arcs of parabola in the zones corresponding to a strand/strand crossing at the top and straight lines elsewhere. The back flattening of the strand is assumed to be centred to the middle of the strand, which is not the case for the side flattening. The crossing surface, simulated by an horse-saddle shape, is symmetrical to the long axis straight-line. The main axes of this surface are the strand axis and the crossing axis (*i.e.* the main axes of the crossing area in the top view). The heights of the strand and the eccentricity of the crossing area are enough to fully defined it. The limit of the contact area is close to an ellipse but, for deeper indentations, it looks more like a diamond. An implicit equation, based on hyperbolic cosines, describes correctly all the behaviours and is fully defined by the long and short axes, the eccentricity and the main angle measured on the top view. The other parts of the strand modelling are assumed to be portions of right cylinder, with the axis parallel to the strand axis. An example of reconstructed strand of a 15 mm width inner cable is shown on fig. 4. Nevertheless, due to the high complexity of the crossing geometry, it is not possible to simulate the complicate shape of the strand at each edge of the cable.

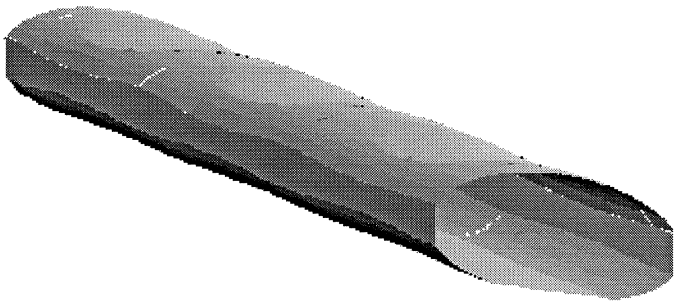

Figure 4: Part of a rebuilt strand for cable 2091

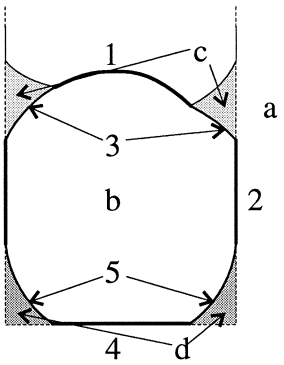

Figure 5: Section of a rebuilt strand: Characteristic areas and volumes

From modelling, we can calculate many parameters which can be estimated only globally by other measurements (or not estimated at all). They are shown in figure 5. Concerning the different areas, we can determine:

1. the contact area between two crossing strands (crossing area),
2. the contact area between two adjacent strands (adjacent area),
3. the free area on the top (inner free area) where exchanges with liquid helium can happen,
4. the flat area on the back (flat back area) in contact with the kapton insulation,
5. the free area on the back (outer free area) in contact either with helium or with insulator.

Concerning the different volumes, we can determine:

a) the volume of the cable envelope,

b) the volume of the strand,

c) the free volume between two crossing strands (inner free volume) where liquid helium can stay,

d) the free volume between a strand and its envelope (outer free volume) where the kapton insulation can flow.

For a better understanding, these parameters are reported on fig 5. Even if the error on these results is difficult to calculate, we can estimate that most of the values are given with an accuracy of 5%, taking into account measurements errors and modelling imperfections.

5. Results for a twist-pitch

Five cables have been studied. The general results presented in the tables B and C are calculated for a twist-pitch.

a. Areas

Table B: Calculated areas for various superconducting cables (per twist-pitch in mm^2)

Cable reference	2136	2180	2191	1B263	2B164
Wire surface before cabling	14165	13814	11037	10879	9912
Wire surface after cabling	14088	13886	10972	11152	9925
Average flat back area	1.40	0.997	0.873	0.843	0.489
Average crossing area	2.02	1.21	1.27	1.17	0.658
Average adjacent area	1.23	0.695	0.783	0.779	0.419
Inner free area	**2999**	**3379**	**2135**	**3054**	**2457**
% of surface after cabling	21.3 %	24.3 %	19.5 %	27.4 %	24.8 %
Outer free area	2746	3996	2910	2394	2310
% of surface after cabling	19.5 %	28.8 %	26.5 %	21.5 %	23.3 %
Cooling efficiency (a. u.)	0.649	0.888	0.711	1.04	1.21

The calculated areas are reported on Table B. The line "Wire surface before cabling" corresponds to the total surface of all the wires used for a twist-pitch and has to be compared with the line "Wire surface" on table A. We see a really good agreement in the results (difference < 2%). The line "Wire surface after cabling" corresponds to the total surface of wire in a twist-pitch so after cabling (sum of areas 1 to 5). There is no clear behaviour between those two parameters: depending on cable, the total surface increases or decreases after cabling. As we expect a systematic behaviour, we can deduce that the change is less than the uncertainty, *i.e.* < 2 % of the initial surface.

The three lines "Average flat back area", "Average crossing area" and "Average adjacent area" correspond to the three different contacts observed on the deformed wire. We notice that there is a constant ratio between the crossing and the flat back areas (1.40 ± 0.05) and between the adjacent and the flat back areas (0.89 ± 0.03), except for cable 2180 (ratio of 1.21 and 0.7 respectively).

Those ratios result probably from the stress distribution inside the cable during the cabling process. A reduction of the compaction decreases also the contact areas whatever is the wire diameter or the number of wires.

The total free surface in a cable varies from 41 % to 55 % of the total surface, inversely to the compaction. It seems also that a smaller compaction induces an higher proportion of free surface inside the cable (~ 26 % for cables 2180, 1B263 and 2B164 compared to ~ 20 % for cables 2136 and 2191). The inner free surface has to be privileged because it surely corresponds to a place of thermal exchange between the wire and the liquid helium, which is not necessarily the case for the outer free surface. We observe that the cables 2180 and 1B263, which have some similar parameters (keystone angle, compaction rate), give similar results. The improvement from design 2191 to design 1B263 is also significant as expected.

Through the heat capacity and the Kapitza resistance, the ratio of the surface of exchange with liquid helium (*i. e.* the inner free area) to the wire volume is a good indication of the "cooling efficiency" of the cable. We observe that cable 2136 and 2191 should be less efficient compared to cables 2180 and 1B263. The outer cable should be the most efficient.

b. Volumes

The calculated volumes are reported in Table C. Due to the fact that some data are extrapolated independently, the total free volume, sum of the inner and the outer free volumes, is not necessarily equal to the difference between the envelope and the wire volumes (difference < 2 %).

Table C: Calculated volumes for various superconducting cables (per twist-pitch in mm^3)

Cable reference	2136	2180	2191	1B263	2B164
Wire volume before cabling	4591	3792	2936	2890	2047
Wire volume after cabling	4644	3827	2994	3066	2060
Envelope volume	5032	4295	3289	3382	2270
Compaction rate	92.3 %	89.1 %	91.0 %	90.6 %	90.8 %
Total free volume	393.3	475.9	298.4	319.5	208.3
Inner volume	**171.3**	**181.5**	**95.6**	**157.1**	**84.1**
% of total free volume	43.6 %	38.1 %	32.0 %	49.2 %	40.4 %
Outer volume	222.0	294.4	202.8	162.4	124.2
% of total free volume	56.4 %	61.9 %	68.0 %	50.8 %	59.6 %
Cooling capacity (a. u.)	3.71	4.77	3.18	5.35	4.14

Confirming a correct calculation, the lines "Wire volume [...]" give similar results and reflect the theoretical value given by the line "Wire volume" in table A. The relatively bad results obtained for cable 1B263 (~5% accuracy compared to ~1% for the other cables) can be attributed to mismeasurements in the wire heights: if the wire is slightly twisted, the back-side is no more horizontal so its shadow can add few tens of micron to the projected profile. Nevertheless, the calculations of wire volume after cabling and envelope volume are so made that this extra-height induces the same extra-quantity in both values. Therefore the difference, which gives the free volume in the cable should not be affected. This is confirmed by the good agreement between each line "Compaction rate" and "Total free volume" of the tables A and C (difference < 10 %).

The repartition of free volumes in the cable varies from cable to cable and no rule related to the compaction can be derived. In most of the cases, insulator flows inside the outer volume and only the inner volume is filled by liquid helium. So, through heat capacity, the ratio of the inner free volume to the wire volume is a good indication of the "cooling capacity" of the cable. Cables 2136 and 2191 should so have a weak cooling capacity regards to cables 2180, 1B263 and 2B164. We observe again similar characteristics between cables 2180 and 1B263 and a significant improvement from design 2191 to design 1B263.

6. Results along an half twist-pitch

We present now the evolution along an half twist-pitch for the most interesting data. By convention in figures, 0 % represent the thick edge and 100 % the thin edge of the cable.

a. Surfaces of contact

The contact areas are interesting to be calculated because these parameters are essential for a good understanding of the inter-strand contact resistance phenomena. They give also an estimation of the force applied in the Turk's head during the cabling process.

Whatever the considered areas, we observe a linear progression along an half twist-pitch of the cable. All the parameters are given on table D and figure 6 shows the curves for the cable 1B263. This is linked to the Turk's head keystone angle: the higher is the keystone angle, the higher are the measured angles but no constant ratio appears. The keystone angle induces a linear distribution of the force along the cable section during the cabling process. Assuming hardness equal to 750 N/mm^2, we estimate through the flat back area values that the force per contact varies from 500 N (thick edge) to 750 N (thin edge) for the cables 2191 and 1B263.

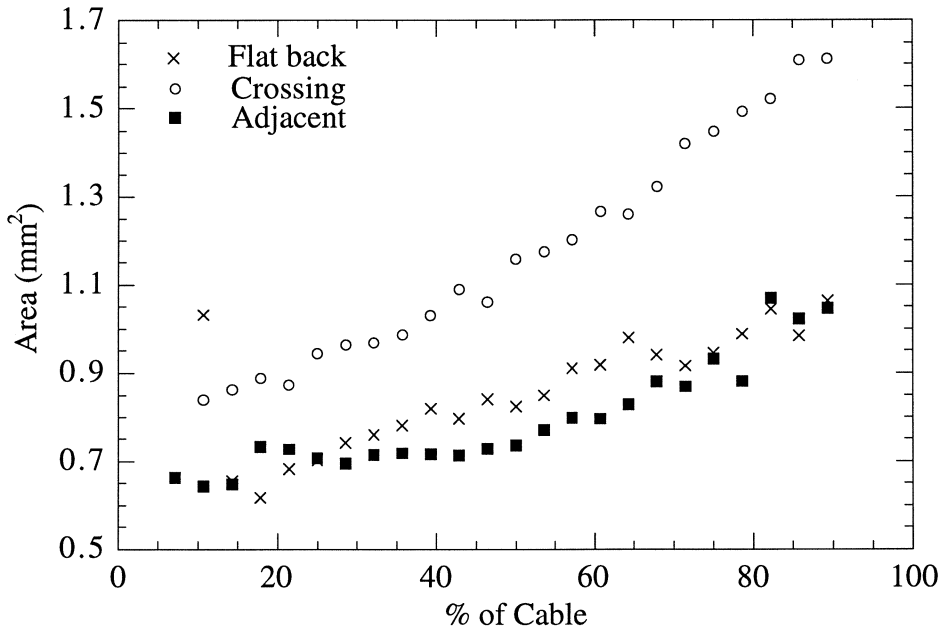

Figure 6: Evolution of the contact areas along an half twist-pitch for the cable 1B263

Table D: Parameter of linear regressions for contact areas

Cable reference		2136	2180	2191	1B263	2B164
Crossing contact	Angle (°)	1.28	0.733	0.848	0.584	0.338
	Value at 0 (mm^2)	0.836	0.568	0.505	0.665	0.365
Adjacent contact	Angle (°)	0.962	0.498	0.665	0.413	0.173
	Value at 0 (mm^2)	0.364	0.274	0.099	0.392	0.252

b. Surface of exchange

We present now the distribution of the inner exchange surface along an half twist-pitch. In all the cases, we observe a linear decrease of the area from the thick to the thin edge. Figure 7 presents the curve for the cable 1B263 and regression parameters are given in table E. For question of periodicity, the values at 0 % (thick edge) and 100 % (thin edge) in the figure have been divided by 2. No evident correlation with the compaction rate or with the keystone angle seems to appear but the cable 1B263 presents a real smaller variation compared to the others. The cables 2136, 2191 and 2B164 show a decrease only from the middle to the thin edge of the cable. A constant area (~ 2.94 mm^2, ~ 1.61 mm^2 and ~ 1.01 mm^2 respectively) is observed in the first half. The stronger compression imposed on the wires near the thin edge of the cable could be the raison for such a behaviour.

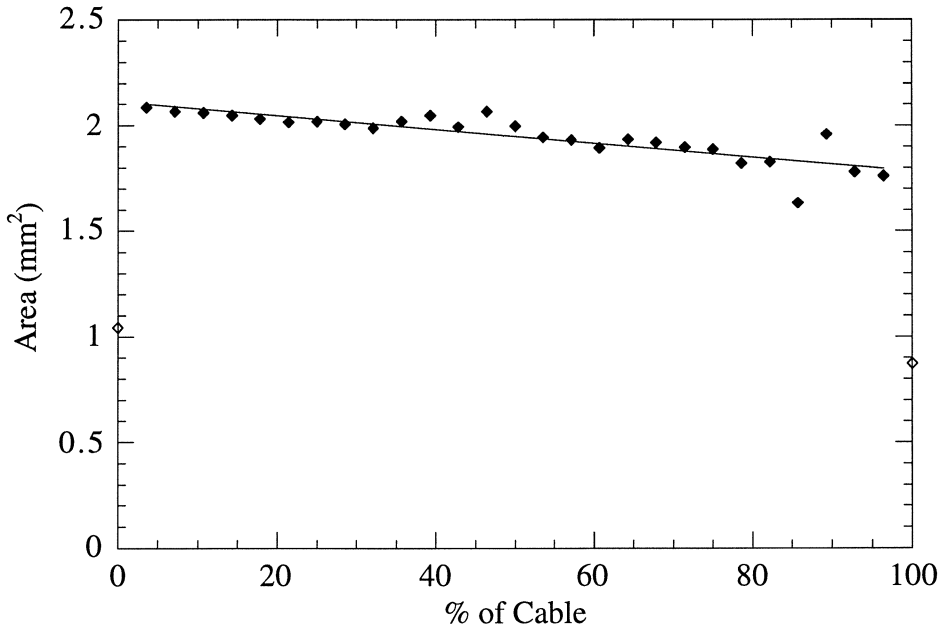

Figure 7: Distribution of the inner exchange surface for the cable 1B263

Table E: Parameter of linear regressions for the inner exchange surface
(*) linear regression observed only for half of the cable

Cable reference	2136 (*)	2180	2191 (*)	1B263	2B164 (*)
Angle (°)	-2.55	-0.796	-0.722	-0.189	-0.470
Value at 0 (mm^2)	4.91	2.57	2.04	2.11	1.42

The cumulative distribution of the inner exchange surface allows us to compare the studied cables to an ideal one (cf. fig 8). It is obtained by integration of the inner exchange surface along the half twist-pitch. For an easier comparison, the integration results are normalized by the total inner exchange surface. The cumulative distribution curve shows so how many percents of the total inner exchange surface are available in a given part of the cable (calculated from the thick edge). From the heat exchange point of view, an ideal cable should have a large exchange area near the thin edge where the cooling has to be the most efficient (this is the nearest edge from the beam and the magnet center).

Unfortunately, the trapezoidal shape of the cable section imposes a decrease of the exchange surface from the thick edge to the thin edge so the ideal situation is when this area remains constant. This is materialised by the straight line in figure 8. We observe that the cable 2136 is the worst case: less than 20 % of the total exchange surface stay in the first third of the cable near the thin edge. The cables 2180, 2191 and 2B164 show a better repartition: ~ 25 % of the surface is used to cool this cable part. The cable 1B263 is close to the ideal repartition.

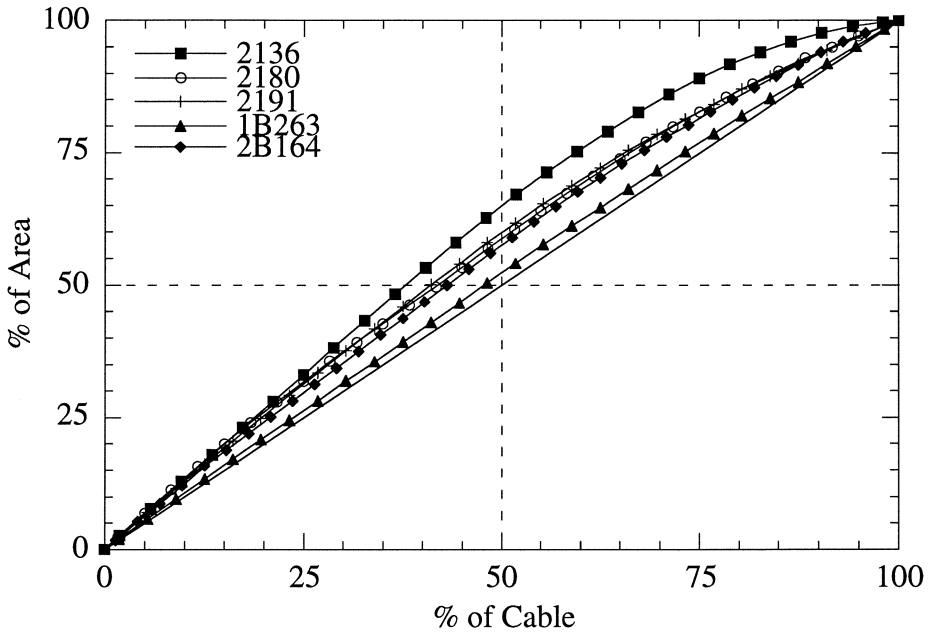

Figure 8: Cumulative distribution of the inner exchange surface

c. Inner free volume

We present now the distribution of the inner free volume along an half twist-pitch. In all the cases, we observe a linear decrease of the volume from the thick to the thin edge. Figure 9 presents the curve for cable 1B263 and regression parameters are given in table F. For question of periodicity, the values at 0 % (thick edge) and 100 % (thin edge) in the figure have been divided by 2. No evident correlation with the compaction rate or the keystone angle seems appear but the cable 1B263 presents a smaller variation compared to the other inner cables. As for the inner exchange surface, the cables 2136, 2191 and 2B164 show two different slopes in their linear regression: a small one from the thick edge to the middle of the cable and a big one (by a factor 2.5 to 4) from the middle to the thin edge. This is probably due to the stronger compression near the thin edge of those cables.

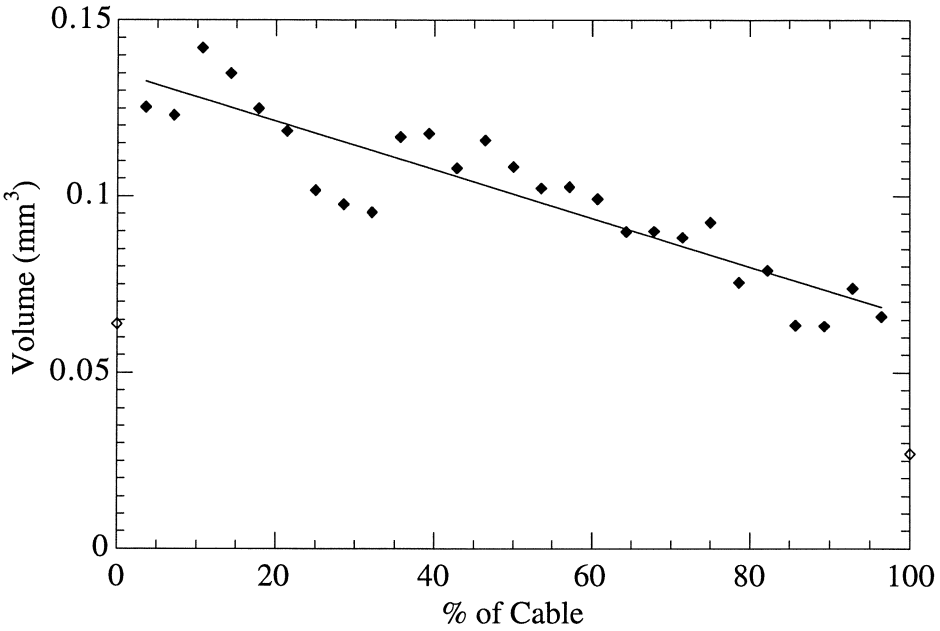

Figure 9: Distribution of the inner free volume for the cable 1B263

Table F: Parameter of linear regressions for the inner free volume
(*) two linear regressions observed on each half of the cable

Cable reference	2136 (*)		2180	2191 (*)		1B263	2B164 (*)	
Angle (°)	-0.056	-0.164	-0.075	-0.024	-0.060	-0.040	-0.008	-0.033
Value at 0 (mm^3)	0.198	0.295	0.170	0.089	0.120	0.135	0.0475	0.065

The cumulative distribution of the inner free volume allows us to compare the studied cables to an ideal one (cf. fig 10). It is obtained by integration of the inner free volume along the half twist-pitch. For an easier comparison, the integration results are normalized by the total inner free volume. The cumulative distribution curve shows so how many percents of the total inner free volume are available in a given part of the cable (calculated from the thick edge). From the thermal stability point of view, an ideal cable should have a large free volume near the thin edge where the cooling capacity has to be high (this is the nearest edge from the beam and the magnet center). Unfortunately, the trapezoidal shape of the cable section imposes a decreasing of the free volume from the thick edge to the thin edge so the ideal situation is when this volume remains constant. This is materialised by the straight line in figure 10. Except cable 1B263 which is close to the ideal case, no large difference in the repartition of the inner free volume appears between the other cables. Only cable 2191 presents a slightly better geometry (more linear so closer to ideal case) compared to the cables 2136, 2180 or 2B164.

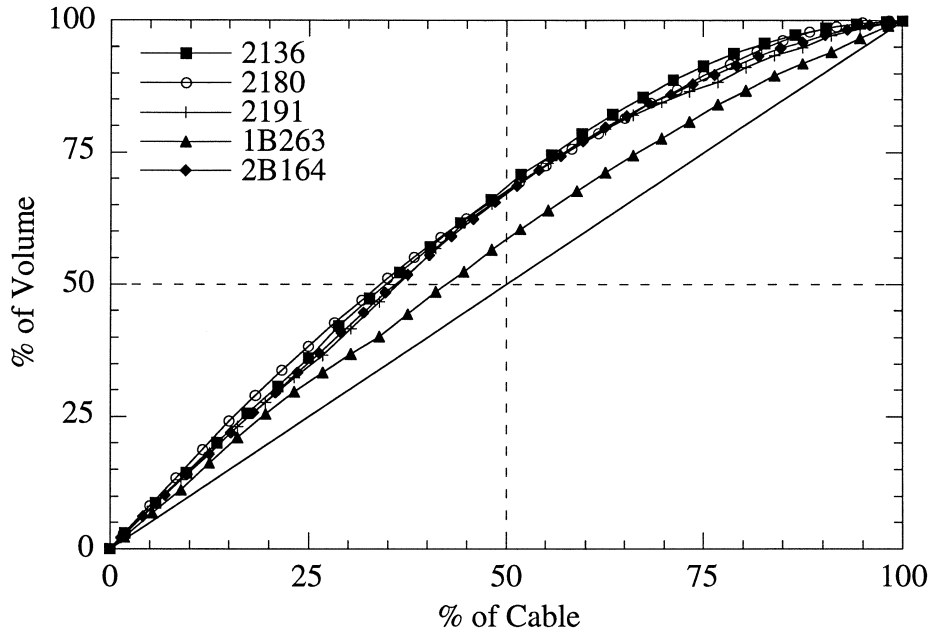

Figure 10: Cumulative distribution of the inner free volume

7. Conclusion

By a profile projection technique we have measured some characteristics of wire extracted from superconducting cables. They have been used in a 3D modelling to rebuild mathematically the deformed wire and to calculate some areas and volumes, fundamental to a correct understanding of the liquid helium circulation inside the superconducting cable. We have for the first time calculated the repartition of the exchange surfaces and the free volumes inside a cable for 5 different designs. Global data (such as total volumes), which can be directly measured by other methods, are consistent together. We have determined two "quality" factors in each case based on the wire volume, the inner exchange area and the free inner volume. The new 15.1 mm width design, improvement of the 15 mm width classical design by transposing some characteristics of the 16.7 mm width design, presents a cable geometry close to the ideal cable and is the best of the 4 studied inner cable designs. The quality factors of the 15 mm width classical outer cable design are good and allow to suppose that the corresponding 15.1 mm width design is also close to the ideal geometry.